Published in final edited form as:
J Neurosci Methods. 2014 November 30; 237: 41–53. doi:10.1016/j.jneumeth.2014.08.023.

A novel slice preparation to study medullary oromotor and autonomic circuits *in vitro*

Jason S. Nasse*
Division of Biosciences, College of Dentistry, 305 West 12th Avenue, 4154 Postle Hall, The Ohio State University, Columbus, OH 43210, United States

Abstract

Background—The medulla is capable of controlling and modulating ingestive behavior and gastrointestinal function. These two functions, which are critical to maintaining homeostasis, are governed by an interconnected group of nuclei dispersed throughout the medulla. As such, in vitro experiments to study the neurophysiologic details of these connections have been limited by spatial constraints of conventional slice preparations.

New method—This study demonstrates a novel method of sectioning the medulla so that sensory, integrative, and motor nuclei that innervate the gastrointestinal tract and the oral cavity remain intact. Results: Immunohistochemical staining against choline-acetyl-transferase and dopamine-β-hydroxylase demonstrated that within a 450 μm block of tissue we are able to capture sensory, integrative and motor nuclei that are critical to oromotor and gastrointestinal function. Within slice tracing shows that axonal projections from the NST to the reticular formation and from the reticular formation to the hypoglossal motor nucleus (mXII) persist. Live-cell calcium imaging of the slice demonstrates that stimulation of either the rostral or caudal NST activates neurons throughout the NST, as well as the reticular formation and mXII.

Comparison with existing methods—This new method of sectioning captures a majority of the nuclei that are active when ingesting a meal. Tradition planes of section, i.e. coronal, horizontal or sagittal, contain only a limited portion of the substrate.

Conclusions—Our results demonstrate that both anatomical and physiologic connections of oral and visceral sensory nuclei that project to integrative and motor nuclei remain intact with this new plane of section.

Keywords

Brainstem; Slice preparation; Oromotor; Calcium imaging; Hypoglossal; Nucleus of the solitary tract

1. Introduction

All life depends upon an organism's ability to obtain an adequate energy supply from its environment and utilize this acquired energy to meet metabolic needs. For mammals this

*Tel.: +1 614 292 4046; fax: +1 614 247 6945. nasse.4@buckeyemail.osu.edu, jasonnasse@yahoo.com.

generally entails seeking out and consuming the appropriate level of nutrients. In order for mammals to respond to changes in metabolic need, multiple sensory signals from the periphery must be processed and integrated to form an appropriate behavioral response. For instance when an animal is hungry, *i.e.* energy deprived, it will seek out nutrients and ingest a meal. Although motivational cues to seek out nutrients are controlled by hypothalamic and forebrain regions, the consummatory phase of a meal, as demonstrated in decerebrate animals, is controlled through circuits in the medulla (Grill and Smith, 1988; Seeley et al., 1994; Grill, 2010; Schneider et al., 2013). Although decerebrate animals do not seek-out food sources, they do maintain the ability to generate and control all phases of consummatory behavior including normal satiety (Grill and Norgren, 1978b).

Integral to controlling ingestive behavior are chemosensory cues from the mouth (reviewed in Travers et al., 1987), and gut (reviewed in Schwartz, 2006). Taste is one cue that can signal the brain as to whether a substance found in the environment may be potentially nutritive or toxic. For example, sweet tasting foods or fluids are generally nutritive and promote ingestion, while bitter tasting food or fluids may signal potentially toxic substances and elicit a rejection response (Grill and Norgren, 1978a). Once a nutritive substance has been ingested, chemo- and mechanosensory mechanisms from the gut initiate the termination of ingestion, i.e. satiety (Smith et al., 1985; Schwartz et al., 1991, 1993; Mathis et al., 1998). While our understanding of these separate but linked systems has grown tremendously in recent years, research as to how the brain integrates these sensory modalities to control consummatory behavior has been limited by a number of factors.

Central control of consummatory behavior and oromotor pattern generation is governed by circuits located in the brainstem and include sensory nuclei (nucleus of the solitary tract, NST), integrative nuclei (medullary reticular formation, mRF), and motor nuclei (dorsal motor nucleus of the vagus (DMN), hypoglossal (mXII), trigeminal motor (mV), and facial motor (mVII) nuclei). These individual nuclei are dispersed throughout the medulla. For instance, vagal afferent fibers from the gut synapse in the caudal nucleus of the solitary tract (cNST) (Rinaman et al., 1989), whereas afferent signals from the tongue synapse in the rostral NST (rNST) (Contreras et al., 1982; Hamilton and Norgren, 1984). The rostral and caudal portions of the NST are separated by approximately 3 mm in the rostro-caudal plane and by 2 mm in the medio-lateral plane. Pre-hypoglossal neurons in the mRF are similarly separated in the rostro-caudal plane but are also dispersed in the dorso-ventral plane at an oblique angle from the midline (Travers et al., 2005). The dispersion of these nuclei pose a challenge when performing slice preparations since the thickness of the slice is a limiting factor in maintaining viable tissue during an experiment. To maintain adequate neuronal viability over the course of an experiment, *in vitro* slice preparations are limited to a thickness of <600 μm (Jiang et al., 1991; Wu et al., 2005). However, slice preparations performed using traditional coronal or horizontal planes of section with a thickness of <600 μm, contain only a limited portion of the substrate involved in orchestrating consummatory behavior in any single section. Therefore, it is impossible to study intact circuits of the oromotor substrate *in vitro* using standard planes of section. This study details a novel method for sectioning the medulla that will, to a large extent, maintain the nuclei and connections that control and/or modulate consummatory behavior within a single 450 μm section of tissue.

2. Materials and methods

2.1. Animals

Sprague-Dawley rat pups with dam (Harlan Industries, Indianapolis, IN) were maintained on a 12:12 light/dark cycle with constant temperature and humidity control. The dam was given *ad libitum* access to both food and water. Pups remained with the dam until the time of each experimental procedure. The use of neonatal rat pups was required for physiologic experiments because the reticular formation becomes heavily myelinated after P12 and hinders the visualization of reticular neurons and the uptake of calcium indicator dyes (Nasse et al., 2008). All experimental procedures were conducted in accordance with National Institutes of Health guidelines, and were approved by The Ohio State University Institutional Animal Care and Use Committee.

2.2. Calculation of angles

To study the functional circuits underlying oromotor and ingestive behaviors with an *in vitro* slice preparation, sensory, integrative, and motor neuronal pools must be contained with the slice. The principal sensory nucleus conveying information from the viscera and oral cavity is the NST. We therefore first determined what angle would be required to achieve the maximum extent of this nucleus in the sagittal plane by orienting the lateral border of the nucleus parallel to the cutting blade. All angle calculations were based on the diagrams of the adult brain atlas: The rat brain in stereotaxic coordinates, 4th edition, by Paxinos and Watson (Academic Press, San Diego, CA, 1998) and subsequently validated using immunohistochemistry and dark-field microscopy. Two angles were considered when determining the oblique orientation: the lateral border of the brainstem and the trajectory of the NST itself. The first angle was determined by drawing a line along the lateral border of the brainstem until it crossed the mid-line just posterior to the spinal medullary junction and measuring the corresponding angle (Fig. 1A). We then determined the angle of trajectory generated by the NST along its lateral border in a similar manner. These two angles were 24° and 30° respectively. The difference of these two angles (6°) was then added to the angle of the NST trajectory (36° total) in order to orient the brainstem such that the lateral border of the NST in the sagittal plane is held parallel to the cutting blade (Fig. 1B). When the medulla is sectioned in this plane, most of the rostro-caudal extent of the NST can be contained in a single 450 μm section (Fig. 2).

Sensory information from the mouth and viscera must be integrated to form appropriate responses based on both taste and metabolic state. Many pre-oromotor neurons innervating the tongue and jaw are located in the medullary reticular formation subjacent to the NST (Travers and Rinaman, 2002; Luo et al., 2006). These pre-oromotor neurons extend ventral and at a slight angle off the midline to a depth of up to 1.5 mm from the ventral border the NST (Travers et al., 2005). In order to include this region in the slice, we measured the angle of trajectory that pre-oromotor neurons follow in the ventro-lateral plane by extending a dividing line between the boundaries of intermediate (IRt) and parvocellular (PCRt) reticular nuclei through the midline dorsal to the brainstem surface (Fig. 1C). We then measured the angle from a line drawn perpendicular to the dorsal surface of the brain and the midline

(55°). This angle was used as the basis for tilting the brainstem at the required pitch to incorporate pre-oromotor neurons along the dorso-ventral axis.

2.3. Tissue holder

Once we determined the angles needed to orient the brainstem in the desired position, wedges of 4% agar were prepared at the measured angles and glued together with cyanoacrylate glue (Loctite 404, Hankle Corporation, Rocky Hill, CT) to form a prototype tissue holder. This holder was then glued to a 22 mm glass microscope slide and placed into a plastic Petri dish filled with a silicon elastomer (Sylard, Dow Corning, Midland, TX) and allowed to cure overnight. The prototype holder was removed from the cured elastomer and discarded. The cured elastomer was then used as a flexible mold that to make holders for future experiments.

To form the holder for individual experiments, melted agar (4%) was poured into the mold and a glass microscope slide is placed over the top. The agar was allowed to solidify at 4 °C for at least 20 min before being removed from the mold and glued to a ceramic block with cyanoacrylate glue. When sectioning, the tissue was placed in the holder such that the left lateral aspect of the brain faces up, and the dorsal surface faces the cutting blade. When gluing the tissue to the holder we found it helpful to puncture a small 1.5 mm hole in the back of the agar holder with a glass pipette prior to putting the tissue in the holder. This acts as an access port to apply the cyanoacrylate glue to the ventral surface of the tissue (Fig. 1D). It is important to keep the placement of glue below the midline. Glue applied too high in front of the tissue can cause damage because sapphire blades do not cut efficiently through hardened glue. Cyanoacrylate glue hardens immediately upon exposure to liquids and tends to float when submersed into the ACSF. Therefore, it is also helpful to briefly immerse the block and tissue inverted into the cutting media before securing it the cutting stage to prevent any excess liquid glue from adhering to the tissue surface when immersing into the cutting media.

2.4. Immunohistochemistry

P9–21 neonatal rats were anesthetized with an overdose ketamine/xylazine and transcardially perfused with 0.1 M phosphate buffered saline (PBS) (pH 7.4) followed by perfusion with ice-cold (4 °C) 4% paraformaldehyde. The tissue was allowed to post fix for 2–24 h and then placed in a 20% sucrose PB solution overnight. Pup brains were then placed into a pre-formed oblique-angle agar holder with the left lateral surface toward the top, and the dorsal surface facing forward. The brain was secured to the holder with cyanoacrylate glue and sectioned just below the mid-line on the rostral side of the tissue with a vibrating tissue slicer (Vibratome Classic-1000) to produce a hemi-section of the medulla in the correct orientation. This tissue block was then mounted onto the stage of a freezing microtome with the cut surface facing down, and sectioned at 40–52 μm.

Tissue sections were rinsed in PBS and antibody labeling was performed against dopamine β-hydroxylase (DBH), choline-acetyltransferase (ChAT), or the purinergic receptor (P2X2) with standard immunohistochemical techniques. Briefly, free floating sections were rinsed 3× in PBS containing 0.02% sodium azide, 10 mg/ml bovine serum albumin and 5% normal

donkey serum (PBS+) (Burry, 2009). Following rinses, the tissue was incubated in PBS+ containing 0.1% Triton-X 100 for 60 min and then rinsed 3 with PBS+ and incubated overnight at room temperature in primary antibodies, mouse anti-DBH (1:7000), and/or goat anti-ChAT (1:100) (Millipore, Billerica, MA) or anti-P2X2 (Alomone Labs, Jerusalem, Isreal). Following several rinses in PBS+ the sections were incubated in secondary antibodies, donkey anti-mouse alexa-fluor 546, and donkey anti-goat 488, for 2–4 h at RT. Sections were then rinsed, mounted on gelatin-coated slides, and cover slipped with vectashield (Vectorlabs, Burlingame, CA) mounting media. Low magnification photomicrographs were taken on a Nikon E800 upright microscope equipped with epifluorescence optics and captured using Nikon, NIS Elements software (Nikon Instruments, Melville, NY).

2.5. Within slice tracing

Neonatal pups aged P9–21 were anesthetized with ethylcarbamate (Urethane) (2 gm/kg) by I.P. injection and euthanized by decapitation. The brain was rapidly removed from the skull and cooled to 4 °C in a modified artificial cerebral spinal fluid (mACSF) containing (in mM) 110 choline chloride, 25 $NaHCO_3$, 2.5 KCl, 7 $MgSO_4 \cdot 7H_2O$, 1.5 NaH_2PO_4, 10 d-glucose, and 0.5 $CaCl_2 \cdot 2H_2O$. The cerebellum was removed and the brainstem was blocked rostrally at the ponto-medullary junction and just caudal to obex. The tissue block was secured to the agar holder described above with cyanoacrylate glue, immersed in ice-cold mACSF, and sectioned with a sapphire blade (Delaware Diamond Knives, Wilmington, DE) on a vibratome. In order to ensure that the correct region of tissue was taken, immunohistochemical experiments were used to map the depth of the lateral border of the NST in relation to the lateral border of the tissue. We determined that this border sits approximately 1 mm below where the blade first makes contact with the tissue. This measurement can be used as a guide to determine when to harvest the 450 μm section of tissue that encompasses the oromotor substrate. Once the tissue is sectioned, the relative translucence of the NST in relation to the more myelinated surrounding tissue is easily observed in pups that are older than P7. If the tissue is sectioned correctly, a single slice will contain the full rostro-caudal extent of the NST.

Following sectioning, the slice was transferred to warmed (32 °C) carboxygenated normal artificial cerebral spinal fluid (ACSF) containing (in mM) 124 NaCl, 25 $NaHCO_3$, 3 KCl, 1 $MgSO_4 \cdot 7H_2O$, 1.5 NaH_2PO_4, 10 d-glucose, and 1.5 $CaCl_2 \cdot 2H_2O$ and allowed to equilibrate for 60 min. Slices were then transferred to a custom-made recording chamber attached to a fixed stage microscope (Nikon E600), and superfused with warm ACSF at a rate of 2 ml/min. Slices were held in place with a custom made gold-wire “harp” strung with elastic nylon strings. The strings of the harp were oriented such that they do not overlay the NST or underlying RF.

Once the slice is secured in the chamber, a small bore (15–30 μm) beveled glass pipette filled with DiI dissolved in ethanol, was directed toward either the rNST ($n = 4$), cNST ($n = 2$), underlying RF ($n = 1$) or the mXII ($n = 1$). A small bolus of DiI was manually injected using light pressure with a 1 ml syringe connected to the pipette. One nucleus per slice was injected and the dye was allowed to track for 1–2 h in the holding chamber before being

removed and fixed in 4% paraformaldehyde overnight. Following overnight fixation the slices were transferred into PBS containing 0.02% sodium-azide, and held at 4 °C for 3–6 weeks to allow enough time for the dye to completely trace axons to the most distal end. Individual sections were imaged with an Olympus, FV1000 multiphoton microscope system. This system allowed us to collect images through the majority of the 450 μm slice without the need to resection the tissue. The collected stacks were further processed with Metamorph imaging software (Molecular Devices, Sunnyvale, CA). Following imaging with the multiphoton microscope, a subset of slices were re-sectioned on a freezing microtome to verify the injection site and nuclei contained in the slice.

2.6. Calcium imaging

Individual sections were cut as described for the within slice tracing studies from pups ranging from P8 to P11. The optimal ages for calcium-imaging experiments utilizing a bath application of the calcium indicator dye are P8–P11, as this range is optimal for the ease of identifying the NST following sectioning and for optimal uptake the calcium indicator dye. After the initial 60 min equilibration time, the sections were incubated in a fluorescent calcium indicator dye solution (Qwest Fluo-8AM or Cal520, ATT-Bioquest,) for 15–20 min in continuously bubbled ASCF at room temperature. The stock dye solution was prepared by dissolving 50 μg of dye into 40 μl, 10% Pluronic-F127 DMSO, and then adding 250 μl ACSF. This stock was pipetted over the tissue and gently mixed in a 22 mm Petri dish containing 3 ml ACSF. The final concentration of dye was approximately 12.5 μM. Following the incubation time, the sections were rinsed 2× for 30 min each, and held at room temperature until imaged. Just prior to imaging, the sections were transferred to a custom made polycarbonate imaging chamber and continuously superfused with warmed (32 °C) carboxygenated ACSF at a rate of 2 ml/min with a peristaltic pump (Dynamax 1000, Rainin Instruments, Oakland, CA). The slices were held in place with a custom-made 22 ga gold-wire harp strung with elastic nylon fibers. Once in the chamber, a concentric bipolar stimulating electrode (World Precision Instruments, Sarasota, FL) was placed in either the rostral (n = 4 slices), caudal (n = 3 slices) or middle (n = 1 slice) NST and used to deliver short (0.5–2.0 s) trains of electric stimulation to the nucleus (50 Hz, 0.1 ms pulses, 200–450 μA). Pulse trains were generated with a Master-8 digital pulse stimulator connected to an ISO-Flex stimulus isolation unit (AMPI, Jerusalem, Israel). Slices were imaged with an Infinity-3 live-cell confocal imaging system (VisiTech International, Sunderland, UK) and data files were digitally stored for off-line analysis. Typical exposure times were 110–150 ms, and images were captured at the maximum frame rate. The calcium indicator dye was excited with a 491 nm LED laser and changes in fluorescent intensity were measured offline using Metamorph Imaging Software (Molecular Devices, Sunnyvale, CA). For each individual slice, the region immediately surrounding the stimulation electrode was imaged first in order to verify slice viability and that little or no movement of the tissue occurred during the stimulation train. Stimulation amplitude was set according to this first observation. Slices were removed from the study if area immediately around the electrode failed to respond to this first stimulation. Following this first stimulation, $GABA_A$ and glycine receptor antagonists SR-95531 and strychnine (5 μM) were added to the media to maximize our ability to detect connected regions within the slice. Starting at the stimulation site, regions responsive to electrical stimulation were systematically recorded with a grid

pattern and individual cells were mapped onto a generic slice diagram to indicate responsive regions in relation to each stimulation site. Individual regions of interest were drawn over responsive cells and the average fluorescent intensity was graphed as a function of time. This response profile was used to categorize the cells into one of six groups (Table 1). The imaging session ended when either the fluorescent signal diminished to the point where adequate signal to noise levels were unattainable, or electrical stimulation was no longer effective at eliciting an increase in fluorescent intensity.

3. Results

3.1. Immunohistochemistry

The first step in validating the oblique method of section was to determine the orientation and extent of the sensory and motor nuclei contained in the slice. In dark-field photomicrographs, both sensory and motor nuclei were easily identifiable based on the morphological differences between sensory and motor regions, and their known spatial relationship to each other in the medulla (Fig. 2A). We used antibody labeling against the P2X2 receptor to help demarcate the extent and boundaries of the NST (Fig. 2B) since the P2X2 receptor is expressed on vagal and facial nerve fibers (Dunn et al., 2001). The boundaries of the NST spanned a maximum distance of 3.2 mm from caudal to rostral within any 52 μm section. P2X2 labeling on the left side NST began approximately 600 μm deep, and continued through to approximately 1240 μm of the tissue. While this distance indicates that some areas of the NST are excluded from our 450 μm span of tissue, the vast majority of P2X2 labeled fibers were evident with only the caudal-most or rostral-most NST regions being excluded depending on the block harvested. We did not observe any systematic differences in orientation of nuclei or extent of the NST captured in the 450 μm thick slice between the different ages used for either immunohistochemical experiments, or with the extent of tracing in the within slice experiments.

The locations of cholinergic and adrenergic/noradrenergic cell groups have been well established in the medulla and served as useful landmarks to further characterize the oblique plane of section (Andén et al., 1965; Levitt and Moore, 1979; Armstrong et al., 1983). Antibody labeling against ChAT and DBH demarcated the boundaries of individual motor pools and adrenergic/noradrenergic cell groups in the brainstem (Fig. 2C). The motor pools for the mV, mVII, mXII and DMN nuclei were at least partially contained with the slice. The A2/C2 and portions of the A1/C1 regions were also observed in the confines of the 450 μm section. The location of these important areas and how they are oriented in the oblique slice was used to determine the depth at which to harvest the section would be most appropriate for neurophysiologic experiments of oromotor circuits.

3.2. In slice tracing

Immunohistochemical studies identified the locations of sensory and motor nuclei in the slice, but did not determine if axonal projection between these nuclei remain intact. We therefore made injections of the lipophilic dye (DiI) directly into regions of interest after sectioning. This allowed us to visualize projections originating from different structures along the oromotor pathway, and served to validate our oblique plane of section for use in

physiologic experiments. Injections made into the rNST revealed axon labeling that traversed caudal within the NTS itself and ventral into the subja-cent RF (Fig. 3A). In some cases, we noted axons that bifurcated within the NST and projected to both caudal NST areas and into the subjacent RF. This may represent a divergence of taste signals to influence multiple brainstem sites. When the cNST was injected with DiI, numerous projections to the subjacent RF (Fig. 3C), as well as toward the rostral NST (Fig. 3D and E) were observed. The fibers emanating from the cNST traversed the entire span of NST that remained in the slice and were measured over a distance of 2.8 mm. This distance is close the maximum span of P2X2 positive fibers that we measured in thin section immunohistochemistry experiments and suggests that connections from both poles of the NST remain intact when the tissue is sectioned at 450 μm. This is a critical point when considering potential gut/taste interactions in an *in vitro* slice preparation because gastric and taste stimuli can reciprocally modulate each other, and intact connections between the rostral and caudal NST further validates the intact nature of the preparation and usefulness in conducting *in vitro* physiologic experiments.

To determine if connections persisted between the reticular formation and mXII we made DiI injections into both regions. Injections of DiI directly into the reticular formation revealed axons that terminated primarily near the region immediately outside of the hypoglossal motor nucleus where dendrites from mXII neurons extend and a few sparse axons in the nucleus itself (data not shown). Injections in mXII labeled relatively few retrogradely traced neurons. While this result may indicate that the connections from the RF to the NST are few in number, subsequent calcium imaging experiments validated that functional connections remain and that rNST stimulation can drive calcium transients in hypoglossal neurons. This demonstrates that projections to mXII from either the rNST or reticular formation do indeed persist after sectioning (see Section 3.3).

3.3. Calcium imaging

Within slice tracing with DiI established that axonal projections to the reticular formation from both the caudal and rostral NST remained after sectioning in the oblique plane. To examine the functional connectivity in the slice, live-cell calcium imaging was used to map functionally connected regions within the slice. Since peripheral sensory signals from the gut and tongue first synapse in the cNST and rNST respectively, we used electrical stimulation of these two regions to map cellular responses along the putative visceral/oromotor circuit. Stimulation of either the cNST or rNST resulted in increased fluorescent intensity in cells throughout most of the slice (Fig. 4). The number of cells that increased fluorescent signal intensity following electrical stimulation was greatest in the regions closest to the electrode. However, stimulation from either the rostral or caudal NST elicited responses in cells that were far removed from the stimulation site. For instance, several cells in mXII responded to stimulation of the rNST ($n = 10$), and large amplitude responses of cNST neurons were also recorded in the same preparation.

The most commonly observed response was a time-locked single-peak increase in fluorescent intensity that decayed shortly following the stimulus (Fig. 5A). In addition to responses that were time-locked to the start of the stimulation, we also observed single-peak

increases that began at a fixed interval after the stimulus began (Fig. 5C) and were consistent with repeated stimulation. This may indicate a polysynaptic pathway to second or third order neurons that was activated by the stimulation. Blocking $GABA_A$ and glycine receptors (SR95531 and strychnine respectively, 5 μM) abolished this delay and potentiated the signal amplitude of this response (Fig. 5D). The number of cells demonstrating an increase in fluorescent signal following electrical stimulation of the NST was greatly increased when $GABA_A$ and glycine receptor antagonists were included in the media, consistent with a previous study performed in coronal slices and stimulating the rNST (Nasse et al., 2008). Therefore, mapping studies included SR95531 and strychnine (5 μM) in the media for the duration of the experiments in order to increase the number of cells activated during each stimulus and maximize our ability to detect connected regions in the slice.

Increases in fluorescent signal show that cells in the slice can be activated, but it does not preclude the possibility of direct or antidromic stimulation of recorded cells. To determine if we were exciting cells through synaptic connections, we blocked ionotropic glutamate receptors in a cNST field that was responsive to rNST stimulation. When ionotropic glutamate receptor antagonists (DNQX and MK-801, 10 μM) were included in the media, increases in fluorescent intensity were completely abolished in all but one cell ($n = 16$). All cells showed at least partial recovery following a 20-min washout period (Fig. 5E and F). This demonstrates that synaptic release of glutamate is the primary mediator of single peak responses, at least in the cNST, of regions distal to the stimulation site.

In addition to the relatively simple single-peak increases in fluorescent intensity, we also observed more complex response types throughout the slice. Several cells were characterized by an initial increase in fluorescent intensity followed by a decrease below baseline that subsequently returned to baseline ($n = 5$). In one instance where ionotropic glutamate receptors were blocked, the initial increase in intensity was abolished, however, the decrease persisted. Following washout, the initial pattern returned. The decrease in this case is of note because $GABA_A$ and glycine receptors were blocked prior to the first stimulus, suggesting an as yet unknown, inhibitory mechanism is responsible for the decrease in signal intensity. Furthermore, several cells demonstrated only a decrease in fluorescent intensity following stimulation ($n = 4$). Detecting decreases in fluorescent intensity is more difficult with calcium imaging because it depends on a high basal level of intra-cellular calcium, perhaps reflecting spontaneous activity. As such, the number of cells with decreased (inhibitory) responses may be an under-representation of the actual number of cells receiving inhibitory input.

We also observed oscillatory changes of fluorescent intensity in both the NST itself and in the underlying reticular formation ($n = 81$). Oscillations were observed in approximately 13.5% of the cells and demonstrated a variety of response profiles. For instance, in some cases stimulation produced a prolonged increase in the calcium signal that rapidly oscillated as the signal returned to baseline (Fig. 6A). In other cells, the stimulation caused a time-locked increase in fluorescent intensity followed by persistent slower oscillations (Fig. 6B). A third group of oscillating cells responded with persistent slow oscillations after the first stimulation, but following a second stimulation the oscillations stopped (Fig. 6C). In a small

percentage of cells (2–4%), stimulation inhibited spontaneous oscillatory activity. The inhibition typically followed a time-locked increase in response to the stimulation, followed by a quiescent period (Fig. 6D).

4. Discussion

4.1. Summary

This study details a novel method for sectioning the medulla that preserves both anatomic and physiologic connections through sensory, integrative, and motor nuclei along the taste/oromotor pathway in a single 450 μm slice. We revealed that projections within the NST are preserved, as well as projections from the NST to the medullary reticular formation, an area where pre-oromotor neurons are located and critical to the generation of consumma-tory oromotor movements (Popratiloff et al., 2001; Travers and Rinaman, 2002; Chen and Travers, 2003). Projections from the reticular formation subjacent to the rNST showed caudally directed projections that entered into and around the hypoglossal motor nucleus. We further demonstrated that electrical stimulation of the either the rostral or caudal NST can activate intracellular calcium mobilization throughout the oromotor pathway, suggesting that the sensory motor circuit remained intact after sectioning. Furthermore, we demonstrated that in addition to time-locked single peak calcium transients, a number of activation patterns were observed, suggesting the induction of network activity following electrical stimulation of the sensory nucleus. These patterns included both the activation and inhibition of oscillatory activity that would be expected with a central pattern generator. In addition, we have demonstrated that blocking either ionotropic glutamate or $GABA_A$ and glycine receptors can modulate or suppress responses to electrical stimulation of the NST.

4.2. Use of neonatal rats

The use of neonatal rats for *in vitro* slice preparations is a common paradigm since they are more amenable to brief bouts of hypoxia and allow greater O_2 penetration than adult sections. This is especially true in areas where the white matter is dense such as the reticular formation (Haddad and Donnelly, 1990; Jiang et al., 1991). Furthermore, because the reticular formation becomes heavily myelinated early during postnatal development, it is nearly impossible to visualize individual neurons in pups that are older than P12 with infrared differential interference contrast optics commonly used with patch clamp experiments. In our experience, fluorescent calcium dyes also are not efficiently taken up by reticular neurons in pups older than P12. These two constraints require the use of young animals for *in vitro* slice preparations that involve medullary reticular neurons and conventional calcium indicator dyes. However, we and others have shown that neonatal animals as early as P5 are able to differentiate between sweet and bitter compounds infused into the oral cavity, i.e. they lick in response to sweet stimuli and gape (reject) in response to bitter stimuli in a similar manner as adult animals (Ganchrow et al., 1986; Nasse and Travers, 2006). Neonatal pups also respond like adult animals when exposed to the satiety peptide CCK (Smith et al., 1991). Therefore, while there are many changes that take place during the first few weeks of development in the rat (Hill et al., 1983; May and Hill, 2006), the neonatal model is useful and valid model for the study of neurophysiologic mechanisms governing a host of ingestive behaviors.

4.3. Alternatives for calcium imaging method

The present study utilized bath application of acetoxymethyl ester (AM) conjugated calcium indicator dyes in order to label neurons throughout the extent of the slice. While this approach has the advantage of labeling cells in all areas of the slice, the AM ester dyes can be to be readily extruded from cells over time, especially when imaged at physiologic temperature (Bootman et al., 2013), which can reduce signal to noise ratios. Furthermore, large diameter neurons may not take up the dye in sufficient quantities to provide adequate signal to noise ratios. However, alternative methods for labeling cells with calcium indicators may be able to overcome these limitations. For instance direct injection of dextran conjugated dyes, which are not as readily extruded for the cytoplasm, directly into regions of interest such as the reticular formation or one or more of the motor nuclei can provide greater dye concentrations in a region of interest (Rogers et al., 2011). Alternatively, retrograde tracing with dextran dyes (O'Donovan et al., 1993) may allow the investigator to increase the age range of animals and may yield superior labeling characteristics in large neurons. In contrast to the use of fluorogenic calcium indicator dyes, genetically encoded calcium indicators (GECIs) put under the control of neuron specific promoters may allow the investigator to utilize older animals when imaging heavily myelinated brain regions and eliminate the loading problems associated with traditional calcium indicator dyes (Shigetomi et al., 2010).

In addition to the limitations of the calcium dyes used in this study, calcium imaging in general has the disadvantage of being most sensitive in detecting excitatory stimuli. Recording inhibitory stimuli can only be achieved in the presence of high basal activity or by stimulating neurons prior the activation of inhibitory pathways. However, the use of electrophysiologic methods such as patch clamp, or by utilizing voltage sensitive dyes or proteins in conjunction with the oblique section are plausible alternatives to calcium imaging methods.

4.4. Functional considerations

The NST is the site of the first synaptic relay for both visceral and oropharyngeal afferents (Contreras et al., 1982; Hamilton and Norgren, 1984; Rinaman et al., 1989). Anterograde tracing studies show that NST efferent pathways travel both rostral and caudal within the NST itself and ventrolaterally into the underlying intermediate and parvocellular reticular formation, as well as other medullary or pontine areas (Cunningham and Sawchenko, 1989; Beckman and Whitehead, 1991; Halsell et al., 1996; Rogers et al., 1999; Streefland and Jansen, 1999; Travers and Hu, 2000; Karimnamazi et al., 2002). These projections course in a loosely organized pattern that follows the trajectory of the NST as it moves off the fourth ventricle from caudal to rostral, and also stream from the lateral border of the NST and traverse ventral in the reticular formation at an angle that is roughly in line with the angle formed by the border of the intermediate and parvocellular reticular formation. In fact, these anatomical features were one of the main considerations taken into account when determining the angle to cut in order to maximize the potential utility of the slice preparation described in this study.

Pre-oromotor neurons of the hypoglossal and trigeminal motor nuclei are located in a column that extends from the pontomedullary junction into the pons (Travers et al., 2005; Luo et al., 2006). Projections from this region are found throughout most of the hindbrain both ipsi- and contra-laterally. The ipsilateral projections between the ponto-medullary junction and obex, i.e. the region spanned by our slice preparation, follow a trajectory similar to those emanating from the rNST (Horst et al., 1991). Studies in our lab have demonstrated synaptic connections between the rNST and pre-oromotor neurons in the subjacent reticular formation (Nasse et al., 2008). However, due to the spatial constraints of conventional slice preparations, until now it has not been possible to demonstrate a functional circuit stemming from the rNST to the hypoglossal motor nucleus *in vitro*. This study demonstrates that stimulation of the rNST increases intracellular calcium in the hypoglossal motor nucleus, and suggests that either a direct projection from the rNST to the hypoglossal motor nucleus, or a circuit from the rNST to the reticular formation and the reticular formation to the hypoglossal motor nucleus persists after sectioning in the oblique plane. This provides the investigator with a substrate to study oromotor pattern generation *in vitro*, which has not previously been possible using traditional planes of section.

Stimulation of taste pathways by intraoral delivery of taste stimuli can modulate visceral and endocrine activity as part of cephalic phase responses (reviewed in Powley, 2000; Kitamura et al., 2010). These cephalic phase responses are mediated to a large extent through the dorsal–vagal complex. The anatomy underlying these cephalic phase reflex arcs includes NST efferent projections onto DMN neurons and direct projections from cranial nerves (reviewed in Laughton and Powley, 1987; Rinaman et al., 1989; Berthoud and Powley, 1990; Powley, 2000). The DMN is the pre-ganglionic parasympathetic motor output for smooth muscle visceral organs and has a viscerotopic columnar organization throughout its rostro-caudal extent (Fox and Powley, 1985). The cephalic phase response would presumably involve multiple regions of the DMN separated along this rostral caudal axis. To date, no neurophysiologic experiments have studied the effects of rostral NST stimulation on these neurons. This is most likely due to limitations in accessing the required substrate *in vitro*; a limitation that can now be over-come. In addition to taste modulation of visceral function, signaling mechanisms from the viscera also modulate responses to taste stimuli. Satiety signals such as gastric distention or the release of CCK decrease rNST responses to sweet stimuli and modulate taste reactivity (Gleen and Erickson, 1976; Giza and Scott, 1983, 1987a, 1987b; Giza et al., 1990, 1992, 1993). These data imply that a yet unknown neurophysiologic mechanism or pathway is in place to modulate the physiologic response to external stimuli based on an animal's metabolic state. Since the afferent projections from the gastric and taste regions of the NST synapse in opposite regions (Contreras et al., 1982; Hamilton and Norgren, 1984; Rinaman et al., 1989), and are reciprocally connected with each other and with the subjacent reticular formation (Horst et al., 1991), the method of sectioning described in this study provides a means to study the neurophysiologic mechanisms that may govern these phenomena *in vitro*.

In addition to oromotor and gastrointestinal function the hind-brain is also responsible for integrating many other autonomic functions that are important for maintaining homeostasis. Among these, and of critical importance to the brain, is the regulation of glucose. Glucose is the primary and essential energy source for the brain, and glucose deprivation, either

through natural or pharmacologic means, elicits feeding and other counterregulatory responses such as corticosterone and glucagon secretion (Borg et al., 1995; Ritter et al., 2001, 2003; Figlewicz et al., 2002). Studies performed in coronal sections have demonstrated neurophysio-logic responses to acute changes in glucose using patch clamp electrophysiology of the cNST (Wan and Browning, 2008) and DMN (Balfour et al., 2006; Wan and Browning, 2008), and demonstrate how low glucose effects individual neurons. The question not answered in these studies however, is what are the effects on downstream neurons or network activity in other important medullary regions such as the rostral areas that are responsive to glucoprivation and are absent in coronal slices. The oblique section modeled here will make it possible to further study the mechanisms that underlie some of these circuits as it contains more of the brainstem substrate that is responsive to glucoprivation.

Both glucoprivic feeding and satiety mechanisms are at least in part mediated by noradrenergic and adrenergic neurons in the medulla (reviewed in Ritter et al., 2006; Rinaman, 2011). The A2 noradrenergic cell group located in the cNST, is innervated by vagal afferents and is potently activated by gastric distention and satiety peptides like CCK and GLP-1 (Smith et al., 1981, 1985; Rinaman et al., 1998; Rogers et al., 2003; Appleyard et al., 2007). Furthermore, ablation of the A2 cell group attenuates the satiety effects of peripheral CCK administration and are consistent in decerebrate models of feeding (Grill and Smith, 1988; Rinaman, 2003). While satiety mechanisms rely on A2 neurons, glucoprivic feeding is associated with the A1/C1 and C2 cell groups, and (although to a lesser extent) the A2 cell group (Ritter et al., 1998, 2001; Hudson and Ritter, 2004). Because our slice preparation contains both of these cell groups, it could possibly serve as an *in vitro* model for the study of these two contrasting behaviors.

The ability to stimulate and record from a dispersed medullary circuit underlying a host of autonomic functions provides a new tool for studying complex systems controlled by the medulla. The new plane of section described in this study combined with live cell calcium imaging has the added benefit of recording many cells simultaneously and may provide a means of observing differential network effects on individual cells that are in close proximity to one another. Additionally, this new slice paradigm could be coupled with newer neurophysiologic tools, such as channelrhodopsin-2, to stimulate genetically identified neurons in the slice and further tease out the mechanisms underlying complex behaviors. Indeed, recent progress in our lab shows promise in combining these two techniques. We have developed a viral vector that rapidly expresses (1–2 weeks) high levels of channelrhodopsin-2(h134r) in neurons expressing the Phox2A/B promoter (Fig. 7). The vector drives high-levels of gene expression throughout the dorsal–vagal complex including DBH positive neurons (Nasse and Travers, 2013). Further more, at the two week time point, numerous projections are seen both emanating from the cNST into the VLM and rNST. Combining these two new techniques provides a powerful new experimental model to further study medullary autonomic circuits *in vitro*.

Acknowledgments

I would thank Alex Toole for providing excellent technical assistance in performing immunohistochemistry and tissue sectioning. I also thank Dr. Joseph B. Travers and Dr. Susan P. Travers for critical reading of the manuscript and suggestions for improvement. This work was supported by National Institutes of Health Grants to Dr. Joseph Travers (DC-00417), and Dr. Susan Travers (DC-004176) and DE 014320.

References

Andén NE, Dahlström A, Fuxe K, Larsson K. Mapping out of catecholamine and 5-hydroxytryptamine neurons innervating the telencephalon and diencephalon. Life Sci. Jul; 1965 4(13):1275–9. [PubMed: 5849269]

Appleyard SM, Marks D, Kobayashi K, Okano H, Low MJ, Andresen MC. Visceral afferents directly activate catecholamine neurons in the solitary tract nucleus. J Neurosci. Nov; 2007 27(48):13292–302. [PubMed: 18045923]

Armstrong DM, Saper CB, Levey AI, Wainer BH, Terry RD. Distribution of cholinergic neurons in rat brain: demonstrated by the immunocytochemical localization of choline acetyltransferase. J Comp Neurol. May; 1983 216(1):53–68. [PubMed: 6345598]

Balfour RH, Hansen AMK, Trapp S. Neuronal responses to transient hypoglycaemia in the dorsal vagal complex of the rat brainstem. J Physiol (Lond). Feb; 2006 570(Pt 3):469–84. [PubMed: 16284073]

Beckman ME, Whitehead MC. Intramedullary connections of the rostral nucleus of the solitary tract in the hamster. Brain Res. Aug; 1991 557(1/2):265–79. [PubMed: 1747757]

Berthoud H-R, Powley TL. Identification of vagal preganglionics that mediate cephalic phase insulin response. Am J Physiol. Feb; 1990 258(2 Pt 2):R523–30. [PubMed: 2178454]

Bootman MD, Rietdorf K, Collins T, Walker S, Sanderson M. Loading fluorescent Ca^{2+} indicators into living cells. Cold Spring Harb Protoc. Feb.2013 (2):122–5. [PubMed: 23378650]

Borg WP, Sherwin RS, During MJ, Borg MA, Shulman GI. Local ventromedial hypothalamus glucopenia triggers counterregulatory hormone release. Diabetes. Feb; 1995 44(2):180–4. [PubMed: 7859938]

Burry, RW. Immunocytochemistry. Springer; 2009.

Chen Z, Travers JB. Inactivation of amino acid receptors in medullary reticular formation modulates and suppresses ingestion and rejection responses in the awake rat. Am J Physiol Regul Integr Comp Physiol. Jul; 2003 285(1):R68–83. [PubMed: 12663257]

Contreras RJ, Beckstead RM, Norgren R. The central projections of the trigeminal, facial, glossopharyngeal and vagus nerves: an autoradiographic study in the rat. J Auton Nerv Syst. Nov; 1982 6(3):303–22. [PubMed: 7169500]

Cunningham ET, Sawchenko PE. A circumscribed projection from the nucleus of the solitary tract to the nucleus ambiguus in the rat: anatomical evidence for somatostatin-28-immunoreactive interneurons subserving reflex control of esophageal motility. J Neurosci. May; 1989 9(5):1668–82. [PubMed: 2470875]

Dunn PM, Zhong Y, Burnstock G. P2X receptors in peripheral neurons. Prog Neurobiol. Oct; 2001 65(2):107–34. [PubMed: 11403876]

Figlewicz DP, Van Dijk G, Wilkinson CW, Gronbeck P, Higgins M, Zavosh A. Effects of repetitive hypoglycemia on neuroendocrine response and brain tyrosine hydroxylase activity in the rat. Stress. Sep; 2002 5(3):217–26. [PubMed: 12186684]

Fox EA, Powley TL. Longitudinal columnar organization within the dorsal motor nucleus represents separate branches of the abdominal vagus. Brain Res. Aug; 1985 341(2):269–82. [PubMed: 4041795]

Ganchrow JR, Steiner JE, Canetto S. Behavioral displays to gustatory stimuli in newborn rat pups. Dev Psychobiol. May; 1986 19(3):163–74. [PubMed: 3709973]

Giza BK, Deems RO, Vanderweele DA, Scott TR. Pancreatic glucagon suppresses gustatory responsiveness to glucose. Am J Physiol. Dec; 1993 265(6 Pt 2):R1231–7. [PubMed: 8285262]

Giza BK, Scott TR. Blood glucose selectively affects taste-evoked activity in rat nucleus tractus solitarius. Physiol Behav. Nov; 1983 31(5):643–50. [PubMed: 6665054]

Giza BK, Scott TR. Blood glucose level affects perceived sweetness intensity in rats. Physiol Behav. 1987a; 41(5):459–64. [PubMed: 3432400]

Giza BK, Scott TR. Intravenous insulin infusions in rats decrease gustatory-evoked responses to sugars. Am J Physiol. May; 1987b 252(5 Pt 2):R994–1002. [PubMed: 3555122]

Giza BK, Scott TR, Antonucci RF. Effect of cholecystokinin on taste responsiveness in rats. Am J Physiol. Jun; 1990 258(6 Pt 2):R1371–9. [PubMed: 2360687]

Giza BK, Scott TR, Vanderweele DA. Administration of satiety factors and gustatory responsiveness in the nucleus tractus solitarius of the rat. Brain Res Bull. Apr; 1992 28(4):637–9. [PubMed: 1617448]

Gleen JF, Erickson RP. Gastric modulation of gustatory afferent activity. Physiol Behav. May; 1976 16(5):561–8. [PubMed: 972948]

Grill HJ. Leptin and the systems neuroscience of meal size control. Front Neuroendocrinol. Jan; 2010 31(1):61–78. [PubMed: 19836413]

Grill HJ, Norgren R. The taste reactivity test. I. Mimetic responses to gustatory stimuli in neurologically normal rats. Brain Res. Mar; 1978a 143(2):263–79. [PubMed: 630409]

Grill HJ, Norgren R. The taste reactivity test. II. Mimetic responses to gustatory stimuli in chronic thalamic and chronic decerebrate rats. Brain Res. Mar; 1978b 143(2):281–97. [PubMed: 630410]

Grill HJ, Smith GP. Cholecystokinin decreases sucrose intake in chronic decerebrate rats. Am J Physiol. Jun; 1988 254(6 Pt 2):R853–6. [PubMed: 3381910]

Haddad GG, Donnelly DF. O_2 deprivation induces a major depolarization in brain stem neurons in the adult but not in the neonatal rat. J Physiol (Lond). 1990; 429(October):411–28. [PubMed: 2126043]

Halsell CB, Travers SP, Travers JB. Ascending and descending projections from the rostral nucleus of the solitary tract originate from separate neuronal populations. Neuroscience. May; 1996 72(1): 185–97. [PubMed: 8730716]

Hamilton RB, Norgren R. Central projections of gustatory nerves in the rat. J Comp Neurol. 1984; 222(4):560–77. [PubMed: 6199385]

Hill DL, Bradley RM, Mistretta CM. Development of taste responses in rat nucleus of solitary tract. J Neurophysiol. Oct; 1983 50(4):879–95. [PubMed: 6631468]

Horst Ter GJ, Copray JC, Liem RS, van Willigen JD. Projections from the rostral parvocellular reticular formation to pontine and medullary nuclei in the rat: involvement in autonomic regulation and orofacial motor control. NSC. 1991; 40(3):735–58.

Hudson B, Ritter S. Hindbrain catecholamine neurons mediate consummatory responses to glucoprivation. Physiol Behav. Sep; 2004 82(2/3):241–50. [PubMed: 15276785]

Jiang C, Agulian S, Haddad GG. O_2 tension in adult and neonatal brain slices under several experimental conditions. Brain Res. Dec; 1991 568(1/2):159–64. [PubMed: 1814564]

Karimnamazi H, Travers SP, Travers JB. Oral and gastric input to the parabrachial nucleus of the rat. Brain Res. Dec; 2002 957(2):193–206. [PubMed: 12445962]

Kitamura A, Torii K, Uneyama H, Niijima A. Role played by afferent signals from olfac-tory, gustatory and gastrointestinal sensors in regulation of autonomic nerve activity. Biol Pharm Bull. 2010; 33(11):1778–82. [PubMed: 21048298]

Laughton WB, Powley TL. Localization of efferent function in the dorsal motor nucleus of the vagus. Am J Physiol. Jan; 1987 252(1 Pt 2):R13–25. [PubMed: 3544872]

Levitt P, Moore RY. Origin and organization of brainstem catecholamine innervation in the rat. J Comp Neurol. Aug; 1979 186(4):505–28. [PubMed: 15116686]

Luo P, Zhang J, Yang R, Pendlebury W. Neuronal circuitry and synaptic organization of trigeminal proprioceptive afferents mediating tongue movement and jaw–tongue coordination via hypoglossal premotor neurons. Eur J Neurosci. Jun; 2006 23(12):3269–83. [PubMed: 16820017]

Mathis C, Moran TH, Schwartz GJ. Load-sensitive rat gastric vagal afferents encode volume but not gastric nutrients. Am J Physiol. Feb; 1998 274(2 Pt 2):R280–6. [PubMed: 9486282]

May OL, Hill DL. Gustatory terminal field organization and developmental plasticity in the nucleus of the solitary tract revealed through triple-fluorescence labeling. J Comp Neurol. Aug; 2006 497(4): 658–69. [PubMed: 16739199]

Nasse J, Terman D, Venugopal S, Hermann G, Rogers R, Travers JB. Local circuit input to the medullary reticular formation from the rostral nucleus of the solitary tract. Am J Physiol Regul Integr Comp Physiol. Nov; 2008 295(5):R1391–408. [PubMed: 18716034]

Nasse J, Travers JB. Solitary nucleus-reticular formation projections in a neonatal slice preparation. Chem Senses. Jun; 2006 31(5):A111–21.

O'Donovan MJ, Ho S, Sholomenko G, Yee W. Real-time imaging of neurons retrogradely and anterogradely labelled with calcium-sensitive dyes. J Neurosci Methods. Feb; 1993 46(2):91–106. [PubMed: 8474261]

Popratiloff AS, Streppel M, Gruart A, Guntinas-Lichius O, Angelov DN, Stennert E, et al. Hypoglossal and reticular interneurons involved in oro-facial coordination in the rat. J Comp Neurol. May; 2001 433(3):364–79. [PubMed: 11298361]

Powley TL. Vagal circuitry mediating cephalic-phase responses to food. Appetite. Apr; 2000 34(2): 184–8. [PubMed: 10744908]

Rinaman L. Hindbrain noradrenergic lesions attenuate anorexia and alter central cFos expression in rats after gastric viscerosensory stimulation. J Neurosci. Nov; 2003 23(31):10084–92. [PubMed: 14602823]

Rinaman L. Hindbrain noradrenergic A2 neurons: diverse roles in autonomic, endocrine, cognitive, and behavioral functions. Am J Physiol Regul Integr Comp Physiol. Feb; 2011 300(2):R222–35. [PubMed: 20962208]

Rinaman L, Baker EA, Hoffman GE, Stricker EM, Verbalis JG. Medullary c-Fos activation in rats after ingestion of a satiating meal. Am J Physiol. Jul; 1998 275(1 Pt 2):R262–8. [PubMed: 9688987]

Rinaman L, Card JP, Schwaber JS, Miselis RR. Ultrastructural demonstration of a gastric monosynaptic vagal circuit in the nucleus of the solitary tract in rat. J Neurosci. Jun; 1989 9(6): 1985–96. [PubMed: 2723763]

Ritter S, Bugarith K, Dinh TT. Immunotoxic destruction of distinct catecholamine subgroups produces selective impairment of glucoregulatory responses and neuronal activation. J Comp Neurol. Apr; 2001 432(2):197–216. [PubMed: 11241386]

Ritter S, Dinh TT, Li A-J. Hindbrain catecholamine neurons control multiple glucoregulatory responses. Physiol Behav. Nov; 2006 89(4):490–500. [PubMed: 16887153]

Ritter S, Llewellyn-Smith I, Dinh TT. Subgroups of hindbrain catecholamine neurons are selectively activated by 2-deoxy-d-glucose induced metabolic challenge. Brain Res. Sep; 1998 805(1/2):41–54. [PubMed: 9733914]

Ritter S, Watts AG, Dinh TT, Sanchez-Watts G, Pedrow C. Immunotoxin lesion of hypothalamically projecting norepinephrine and epinephrine neurons differentially affects circadian and stressor-stimulated corticosterone secretion. Endocrinology. Apr; 2003 144(4):1357–67. [PubMed: 12639919]

Rogers RC, Hermann GE, Travagli RA. Brainstem pathways responsible for oesophageal control of gastric motility and tone in the rat. J Physiol (Lond). Jan; 1999 514(Pt 2):369–83. [PubMed: 9852320]

Rogers RC, McDougal DH, Hermann GE. Leptin amplifies the action of thyrotropin-releasing hormone in the solitary nucleus: an in vitro calcium imaging study. Brain Res. Apr.2011 1385:47–55. [PubMed: 21334313]

Rogers RC, Travagli RA, Hermann GE. Noradrenergic neurons in the rat solitary nucleus participate in the esophageal–gastric relaxation reflex. Am J Physiol Regul Integr Comp Physiol. Aug; 2003 285(2):R479–89. [PubMed: 12714355]

Schneider JE, Wise JD, Benton NA, Brozek JM, Keen-Rhinehart E. When do we eat? Ingestive behavior, survival, and reproductive success. Horm Behav. Sep; 2013 64(4):702–28. [PubMed: 23911282]

Schwartz GJ. Integrative capacity of the caudal brainstem in the control of food intake. Philos Trans R Soc Lond B: Biol Sci. Jul; 2006 361(1471):1275–80. [PubMed: 16874932]

Schwartz GJ, McHugh PR, Moran TH. Gastric loads and cholecystokinin synergistically stimulate rat gastric vagal afferents. Am J Physiol. Oct; 1993 265(4 Pt 2):R872–6. [PubMed: 8238459]

Schwartz GJ, Netterville LA, McHugh PR, Moran TH. Gastric loads potentiate inhibition of food intake produced by a cholecystokinin analogue. Am J Physiol. Nov; 1991 261(5 Pt 2):R1141–6. [PubMed: 1951762]

Seeley RJ, Grill HJ, Kaplan JM. Neurological dissociation of gastrointestinal and metabolic contributions to meal size control. Behav Neurosci. Apr; 1994 108(2):347–52. [PubMed: 8037879]

Shigetomi E, Kracun S, Sofroniew MV, Khakh BS. A genetically targeted optical sensor to monitor calcium signals in astrocyte processes. Nat Neurosci. Jun; 2010 13(6):759–66. [PubMed: 20495558]

Smith GP, Jerome C, Cushin BJ, Eterno R, Simansky KJ. Abdominal vagotomy blocks the satiety effect of cholecystokinin in the rat. Science. Aug; 1981 213(4511):1036–7. [PubMed: 7268408]

Smith GP, Jerome C, Norgren R. Afferent axons in abdominal vagus mediate satiety effect of cholecystokinin in rats. Am J Physiol. Nov; 1985 249(5 Pt 2):R638–41. [PubMed: 4061684]

Smith GP, Tyrka A, Gibbs J. Type-A CCK receptors mediate the inhibition of food intake and activity by CCK-8 in 9- to 12-day-old rat pups. Pharmacol Biochem Behav. 1991; 38(1):207–10. [PubMed: 2017446]

Streefland C, Jansen K. Intramedullary projections of the rostral nucleus of the solitary tract in the rat: gustatory influences on autonomic output. Chem Senses. Dec; 1999 24(6):655–64. [PubMed: 10587498]

Travers JB, Rinaman L. Identification of lingual motor control circuits using two strains of pseudorabies virus. Neuroscience. 2002; 115(4):1139–51. [PubMed: 12453486]

Travers JB, Travers SP, Norgren R. Gustatory neural processing in the hindbrain. Annu Rev Neurosci. 1987; 10:595–632. [PubMed: 3551765]

Travers JB, Yoo J-E, Chandran R, Herman K, Travers SP. Neurotransmitter phenotypes of intermediate zone reticular formation projections to the motor trigeminal and hypoglossal nuclei in the rat. J Comp Neurol. Jul; 2005 488(1):28–47. [PubMed: 15912497]

Travers SP, Hu H. Extranuclear projections of rNST neurons expressing gustatory-elicited Fos. J Comp Neurol. Nov; 2000 427(1):124–38. [PubMed: 11042595]

Wan S, Browning KN. d-Glucose modulates synaptic transmission from the central terminals of vagal afferent fibers. Am J Physiol Gastrointest Liver Physiol. Mar; 2008 294(3):G757–63. [PubMed: 18202107]

Wu C, Luk WP, Gillis J, Skinner F, Zhang L. Size does matter: generation of intrinsic network rhythms in thick mouse hippocampal slices. J Neurophysiol. Apr; 2005 93(4):2302–17. [PubMed: 15537814]

HIGHLIGHTS

- We have developed a new way of sectioning the medulla for *in vitro* studies.
- The slice encapsulates sensory, integrative, and motor nuclei for oromotor control.
- Axonal connections were validated with both tract tracing and live-cell imaging.
- Neurons in integrative and motor nuclei were activated by sensory area stimulation.
- The slice serves as an *in vitro* model to study oromotor and autonomic pathways.

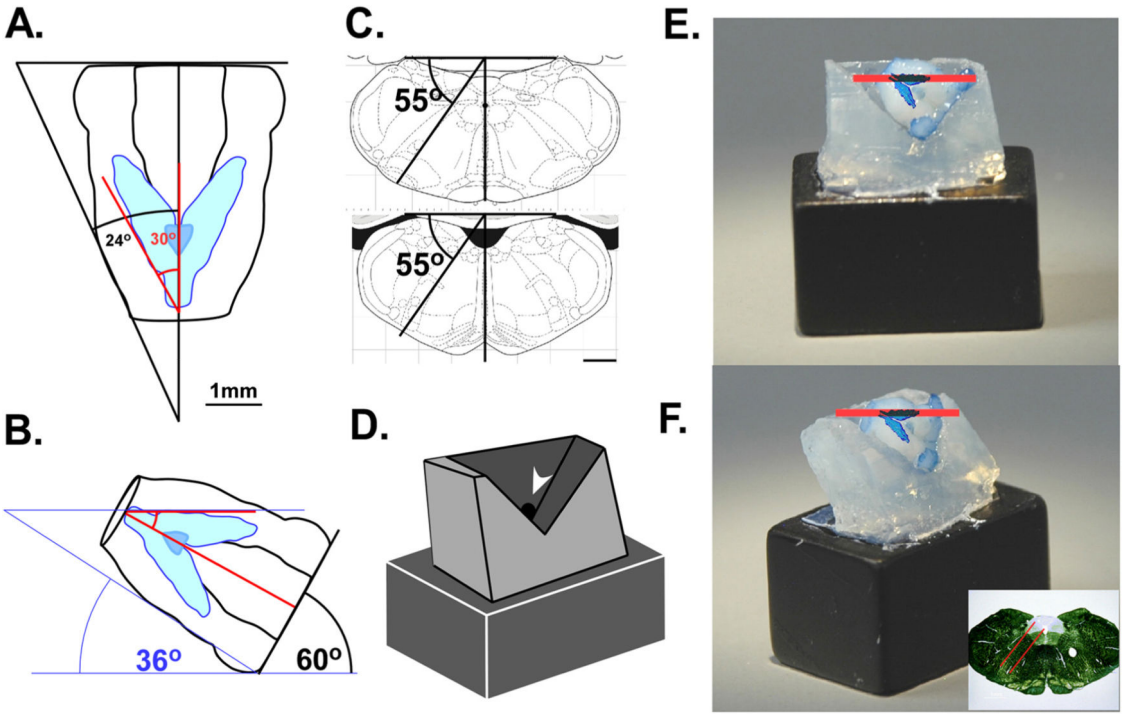

Fig. 1.

(A) To orient the tissue so that the lateral border of the left NST is parallel to the cutting the plane, the difference between the angle of the outside of the tissue (24°) and the angle of the NST trajectory was added to the angle of the NST trajectory (36°). (B) Diagram of the brainstem orientation held at 36° showing the lateral border of the left NST held parallel to the cutting plane (red line). (C) Diagram of the angle formed by the boundaries of the IRt where most pre-oromotor neurons are located; this oblique angle also corresponds to a major functional axis of the RF. Scale bars = 1 mm. (D) Schematic diagram of the agar holder indicating location of port punctured through the block (arrow) for application of glue; the angle formed by the "V" corresponds to the 90° angle between where the tissue is blocked and the lateral surface of the brain. (E) View of the agar holder glued to a ceramic block in the oblique angle (right) and facing the cutting blade (left) with a fixed brain glued in place to show the proper orientation. A scaled diagram of the NST is overlaid onto the photographs to show its alignment in relation to the cutting blade. The red bar shows the plane of section and an approximate 450 μm width. The inset shows the cutting angle and approximate slice thickness in the coronal plane. (For interpretation of the references to color in this figure legend, the reader is referred to the web version of the article.)

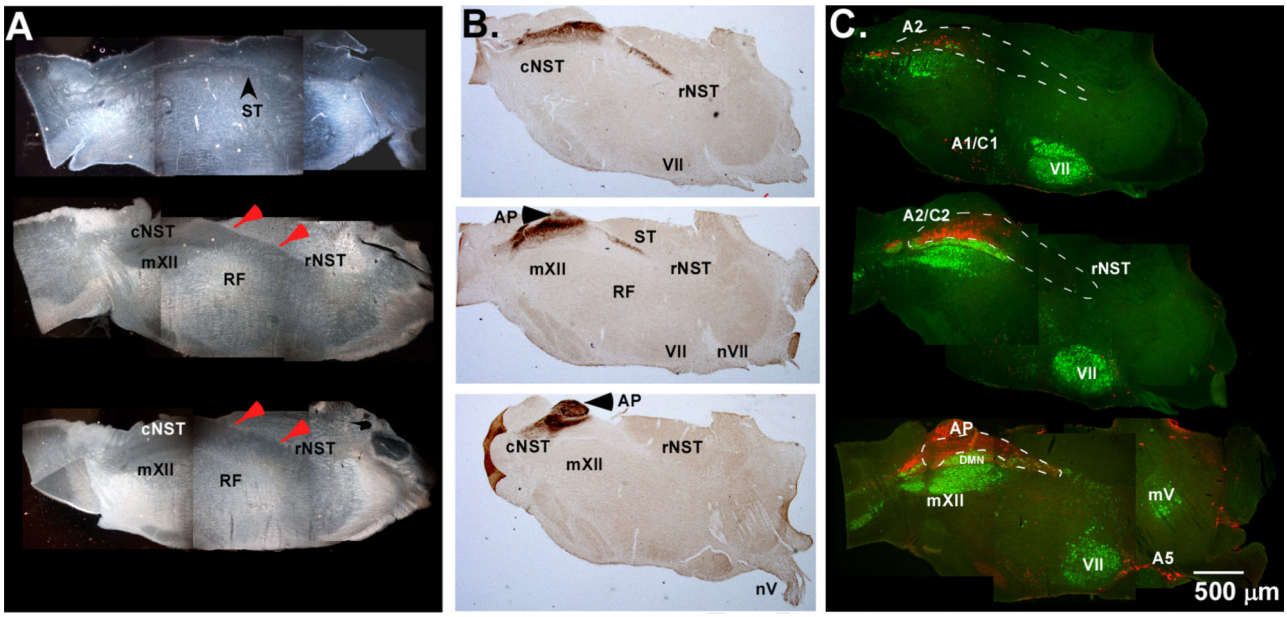

Fig. 2.

(A) Dark-field photomicrographs of sectioned tissue spanning an approximately 450 μm depth through the tissue. The top section is the most lateral aspect and the bottom section is the most medial. Red arrows point to dorsal border of the NST. (B) Antibody labeling of P2X2 receptors demarcates incoming afferent fibers from cranial nerves V, VII, and X and is used to indicate the location of the solitary tract and a portion of the NST that receives primary afferent taste and visceral afferents. (C) Antibody labeling for ChAT (green) and DBH (red) shows the location of cranial motor pools (mXII, VII, and mV), and adrenergic/noradrenergic cells groups housed within the slice. AP: area postrema; cNST: caudal nucleus of the solitary tract; mXII: hypoglossal motor nucleus; mV: trigeminal motor nucleus; VII: facial motor nucleus; nV: facial nerve rootlet; rNST: rostral nucleus of the solitary tract; RF: medullary reticular formation; ST: solitary tract; A2/C2: A2/C2 noradrenergic cell groups.

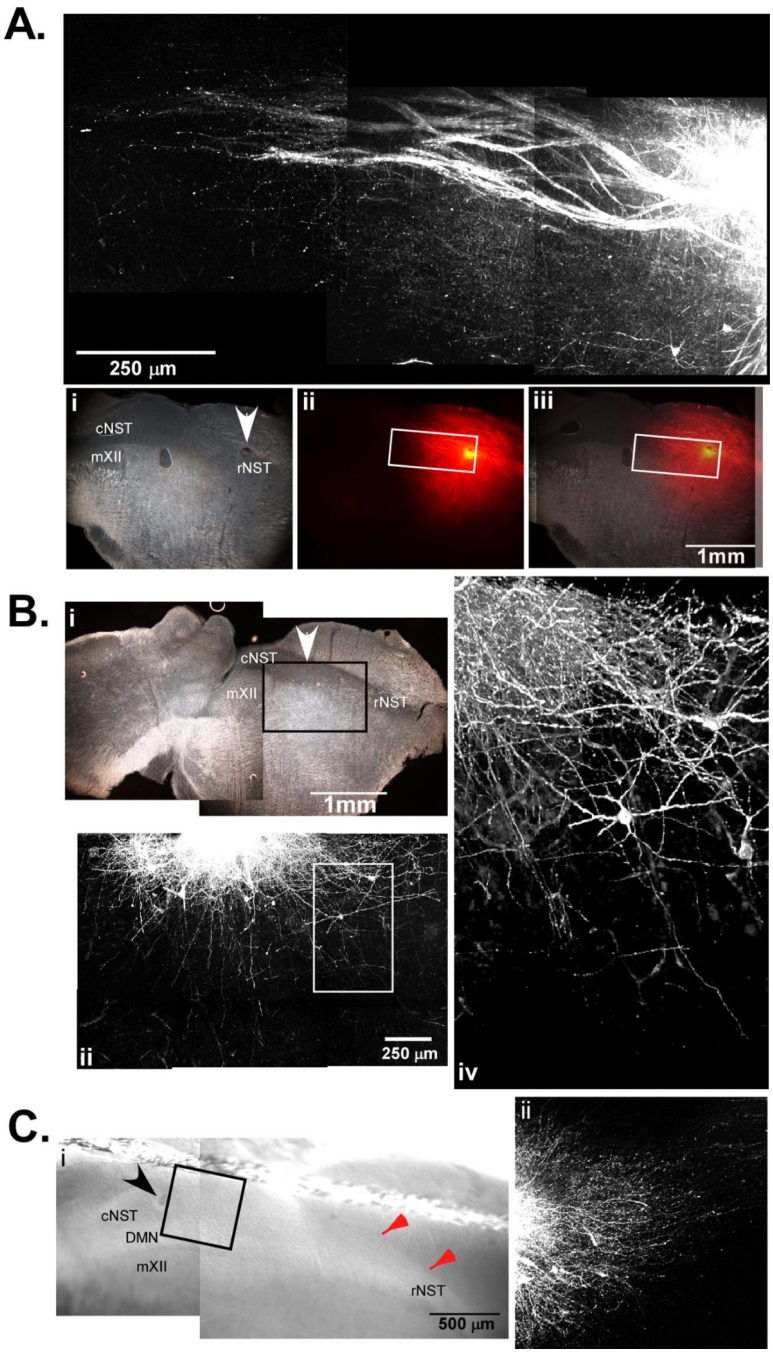

Fig. 3.

(A) Photomicrograph if the rNST following an injection of DiI into rNST in a 450 μm oblique section. The area around the DiI injection site was imaged with a multiphoton confocal microscope to a depth of approximately 300 μm. Axonal projections course through the NST in the caudal direction as well as into the underlying reticular formation. The visible fibers in this case spanned a distance of approximately 1.2 mm from the center of the injection site. Dark-field photomicrograph (i) of the same tissue sectioned at 40 μm showing the injection site (arrow) and nuclei contained in the slice. The middle column (ii)

is fluorescent photomicrograph of the same tissue section. Fibers were seen projecting away from the injection site into the cNST and the subjacent RF. The white box indicates the area imaged with the multiphoton microscope. (B) Photomicrograph taken of a case where DiI was injected into intermediate NST (arrow) in a 450 μm tissue block, and re-sectioned on a freezing microtome at 40 μm (i). The area around the DiI injection site was imaged with a multiphoton confocal microscope prior to re-sectioning to a depth of approximately 300 μm (ii). Axonal projections are seen infiltrating the underlying reticular formation and projecting in the direction of the rNST. On the right (iv) is a 3D projection of the area in the white box at a higher magnification showing axons running into the reticular formation. (C) Photomicrograph of the section just after DiI injection into the cNST and prior to fixation, a “harp” string in seen running above the dorsal border of the NST (red arrows). On the right is a photomicrograph of DiI labeled fibers coursing rostral within the NST. (For interpretation of the references to color in this figure legend, the reader is referred to the web version of the article.)

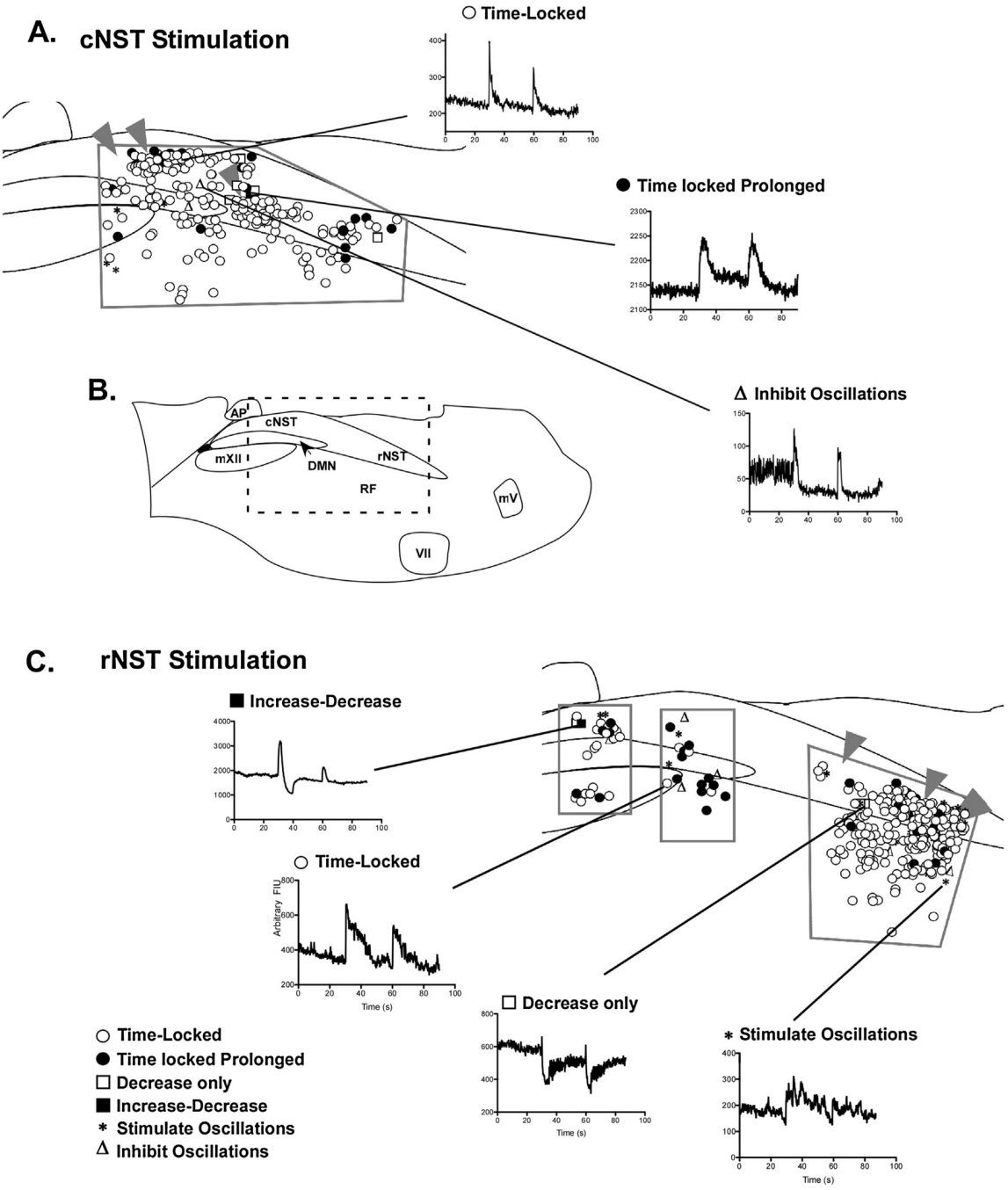

Fig. 4.

Diagrammatical representation of location and response types of cells categorized in calcium imaging experiments. All characterizations and mapping were performed with SR95531 and strychnine in the media. (A) Diagram of responses observed when stimulating the cNST (arrowheads are the location of the stimulating electrode). The regions imaged for mapping experiments are outlined in gray. (B) Diagram of the slice indicating the location and putative boundaries of nuclei housed within the slice. The box denotes the area depicted in (A) and (C). (C) The lower panel diagrams response types observed with stimulation of the

rNST (arrowheads). The area imaged for mapping experiments is outlined in gray. Representatives for each response type (Table 1) are shown between both (A) and (C).

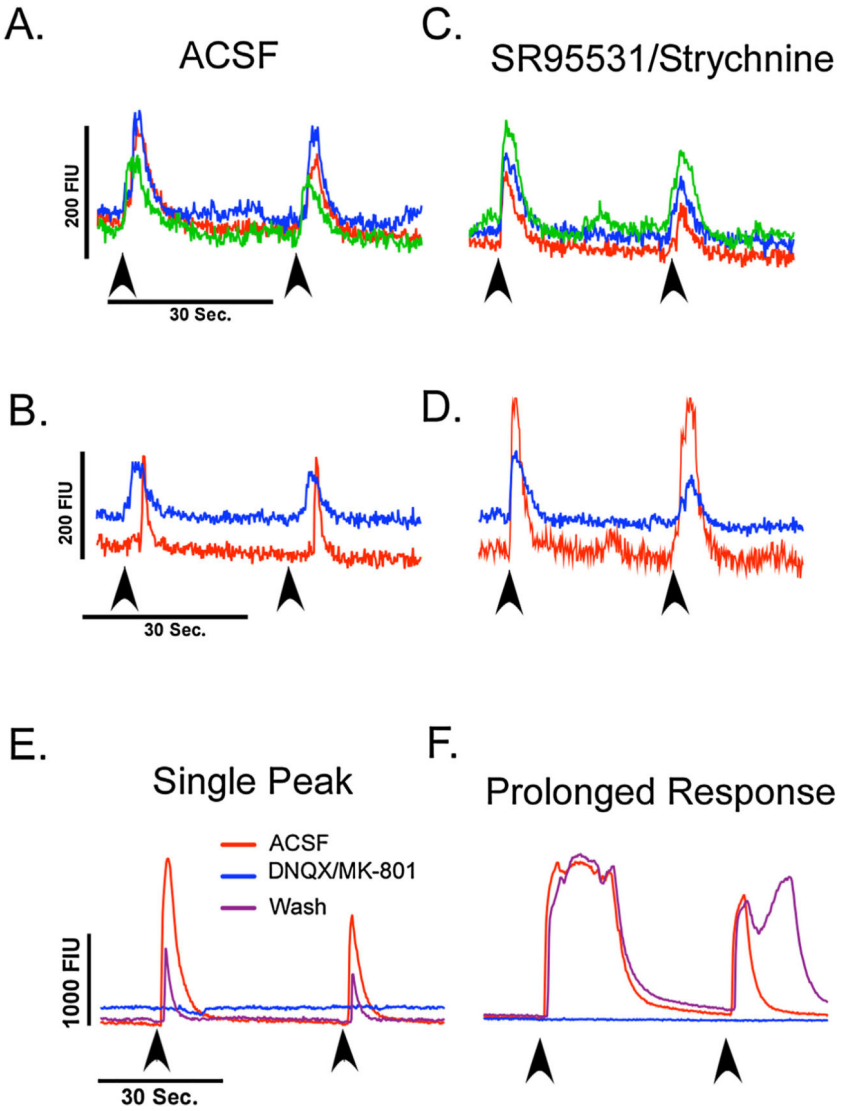

Fig. 5.

(A) Representative traces from three cells recorded simultaneously demonstrating a time-locked increase in fluorescent activity following electrical stimulation of the NST in normal ACSF. (B) Representative trace of cells in the same field that demonstrated a delayed response to electrical stimulation (red trace) and time-locked response (blue trace). Arrows indicate the stimulation onset. (C) When $GABA_A$ and glycine receptors were blocked with SR95531 and strychnine (5 μM), no change was seen in cells that had time-locked responses. (D) The cell that had a delayed response however, became time-locked to the stimulus and had an increased amplitude in fluorescent intensity. (E and F) Representative traces of cells in the cNST that were activated by rNST stimulation (red trace). Ionotropic glutamate receptor antagonists (DNQX and MK-801, 10 μM) abolished the increases in fluorescent intensity (blue trace) that recovered following washout (purple trace). (For interpretation of the references to color in this figure legend, the reader is referred to the web version of the article.)

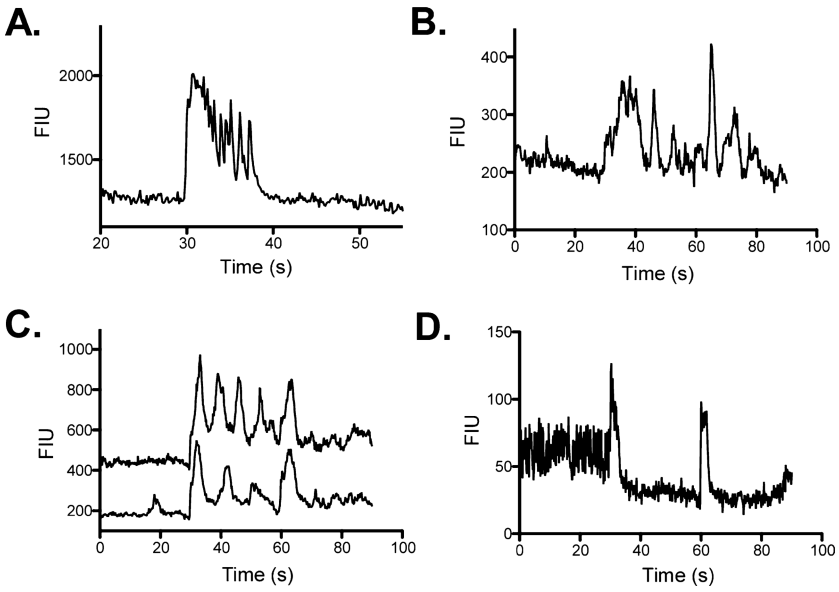

Fig. 6.

Representative examples of cells that responded with oscillatory changes in fluorescent intensity following NST stimulation. (A) Response type categorized by an initial time-locked increase in fluorescent intensity followed by rapid oscillations as the signal returned to baseline. (B) Following the initial response, this cell type demonstrates repeated oscillations with amplitudes similar to the initial stimulus response. (C) This cell type began oscillating after the first stimulus; however, oscillatory activity was inhibited following the second stimulation. (D) This cell type presented with oscillatory activity prior to stimulation that was inhibited by the stimulation.

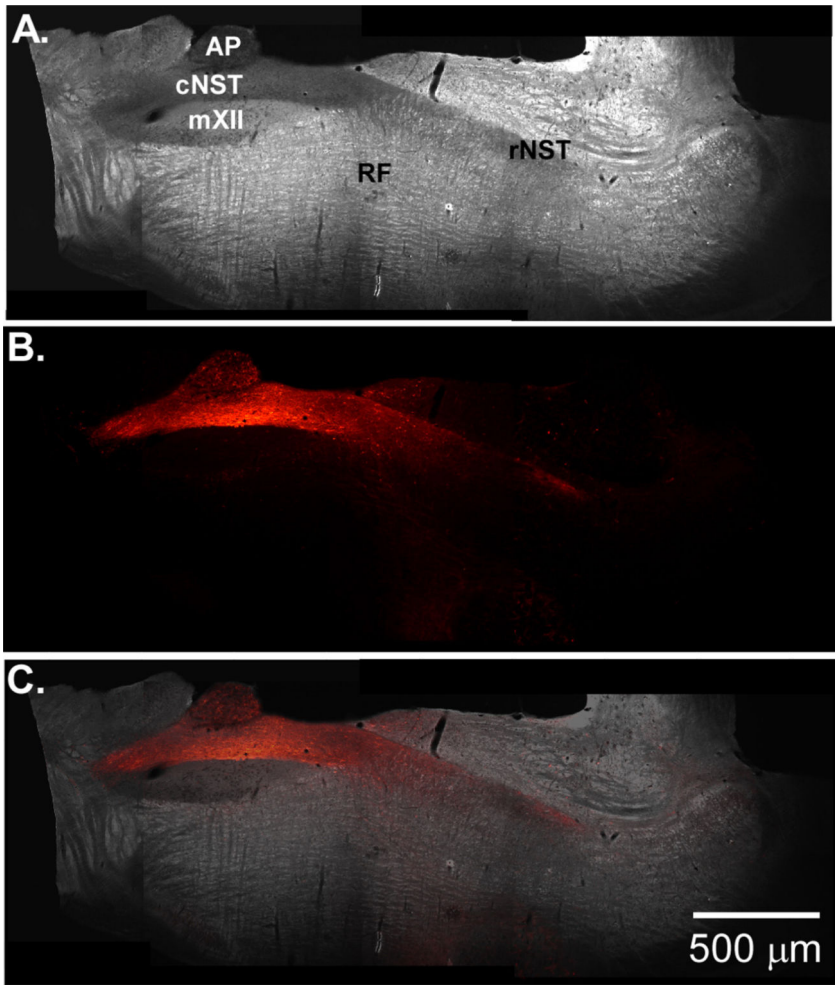

Fig. 7.

(A) Dark-field photomicrograph of oblique section from rat pup injected with an adeno-associated viral vector that expresses a channelrhodopsin-2(h134r)-mCherry fusion protein under the control of the synthetic promoter PRSx8 (Nasse and Travers 2013). (B) Fluorescent photomicrograph of the same slice showing transfected cells in the cNST and fibers projecting to the rNST and reticular formation. (C) Overlay of (A) and (B).

Table 1

Stimulation site	Pups N	Cells N	Two responses	Time-locked	Prolonged	Decrease	Induce oscillation	Inhibit oscillation
cNST	3	207	10.63%	83.09%	12.08%	0.97%	14.49%	1.45%
Mid-NST	1	81	11.11%	98.77%	0.00%	1.23%	11.11%	0.00%
rNST	4	320	10.63%	74.69%	20.00%	1.25%	13.13%	3.75%